Measurements of Large-Scale Parameters of a Distributed MIMO Antenna System in a Microcell Environment at 2.6 GHz

Flordelis, Jose; Dahman, Ghassan; Tufvesson, Fredrik

Published in:
Antennas and Propagation (EuCAP), 2013 7th European Conference on

2013

Measurements of Large-Scale Parameters of a Distributed MIMO Antenna System in a Microcell Environment At 2.6 GHz

Jose Flordelis, Ghassan Dahman and Fredrik Tufvesson
Dept. of Electrical and Information Technology, Lund University, Lund, Sweden
Email: *firstname.lastname*@eit.lth.se

***Abstract*—Multi-site multi-antenna measurements for semi-urban microcell environment at 2.6 GHz are performed with four base stations (BSs) and one mobile station (MS). Three BSs are provided with four antenna elements in closely spaced co-polarized configuration, and one BS is provided with a single antenna element. The MS is equipped with a cylindrical uniform array consisting of 64 dual-polarized antenna elements and moves along some predefined routes. The values of large-scale fading (LSF) from 19 measurement runs with a total of 1900 snapshots at different locations are extracted. The cross-correlation properties of the LSF between different BS links are analyzed. It was found that, in the selected propagation environment, the influence of the BS location on the LSF cross-correlation properties is negligible. However, the location of the MS has a significant influence on the LSF cross-correlation properties of the different BS links.**

***Index Terms*—multi-site, MIMO measurements, large-scale parameters, cross-correlation, distributed MIMO.**

I. Introduction

Wireless radio channels are known for their complex, random spatiotemporal variations. The difficulty in estimating the exact details about a channel realization at a specific location presents a real challenge in the development of accurate channel models that can be used to evaluate the performance of multiple antenna systems. Besides the randomness of radio channels that comes from the interacting objects (IOs) in the propagation environment due to scattering, reflection and diffraction phenomena, the time- and space-varying nature of the channel increases the complexity of the modeling effort.

Multi-antenna channel models adopt different approaches in order to simplify, yet efficiently model, this spatiotemporal random behavior of the wireless link. For example, in the geometry-based stochastic channel models (GSCM) such as COST 2100 [1] and WINNER [2], the parameters of each multi-path component, e.g. power, delay, angle of arrival, angle of departure, are selected randomly from appropriate distributions. These distributions are determined according to global or large-scale parameters (LSPs), which describe the characteristics of the channel over a relatively large area (called a *simulation drop* or *segment*) in the order of a few tens of wavelengths. Modeling the LSPs in a single MIMO link as well as the correlation among them has been the main target of several research works [3] [4], which have been adopted by the 3GPP spatial channel model (SCM), COST 2100 and WINNER models.

In the future, different forms of distributed multi-antenna systems will be used to further improve the performance of communication systems. The use of distributed multi-antennas allows the receiver to process the signal received from a single or multiple propagation links simultaneously. Because of the possibility of having common IOs contributing to different links, the parameters describing different links may exhibit certain correlation [5]. In macrocell environments, correlation among LSPs of different links and its impact on capacity have been investigated in several papers. The investigation includes studying: the correlation among delay spreads, angular spreads, and shadow fading of different links [4], the correlation properties of shadow fading as a function of angle between base stations [6], and the effect of link power imbalances on the perception of LSPs [7] as well as on system capacity [8]. Not enough studies have been performed to model the LSPs of different MIMO links and to model the correlation among them in microcellular environments. In [9], measurements were used to study the spatiotemporal structure of different MIMO links in a microcell environment, though the base stations (BSs) were placed above rooftops. It is expected that the effect of correlation among the LSPs, especially the large-scale fading (LSF), of different links on system capacity will be more pronounced in the case of microcells when the height of the transmit antennas is lower than the surrounding buildings.

The goal of this work is to study the LSF cross-correlation properties of different BS-MS links. This is done by performing simultaneous measurements of MIMO links between four transmit antenna sites, placed lower than the surrounding buildings, and one mobile station (MS) in a microcellular environment at 2.6 GHz. The measured MIMO channels are used to extract the LSF of the individual links. Then the effect of the BS location and the MS location on the cross correlation characteristics of LSF among the different links is studied.

The remainder of this paper is organized as follows: in Secions II and III the measurement setup and the measurement scenario are described. Section IV presents a method for extracting LSF from raw data. Results on the cross-correlation of LSF in a multi-link environment are reported in V.

978-88-907018-1-8/13/$31.00 ©2013 IEEE

TABLE I
SUMMARY OF MEASUREMENT PARAMETERS.

Parameter	Symbol	Value
center frequency (GHz)	f_c	2.570
bandwidth (MHz)	B	40
transmit power (dBm)	P_{TX}	30
number of transmit elements	M_T	13
number of receive elements	M_R	64
signal length (μs)	L	12.8
frequency bins	N	513
snapshot distance (λ_c^{-1})	δ	0.25...0.50

TABLE II
LIST OF PARTS USED FOR THE MEASUREMENTS.

BS	Tx Units	RoF Trx	Fiber (m)	RF PA
BS E	1–4	N/A	-	ZVE-8G-7+, ZHL-42
BS S	5	OZ816	1613	ZVE-8G-7+
BS F	6–9	OZ816	1173	ZVE-8G-7+
BS M	10–13	OZ816	1629	ZVE-8G-7+

Fig. 1. (Left) MS antenna with 64 dual-polarized patch antenna elements. (Top right) BS ULA antenna with 5 dual-polarized patch antenna elements. (Bottom right) Transmitter module showing an OZ816 optical receiver unit and the ZVE-8G-7+ RF power amplifier.

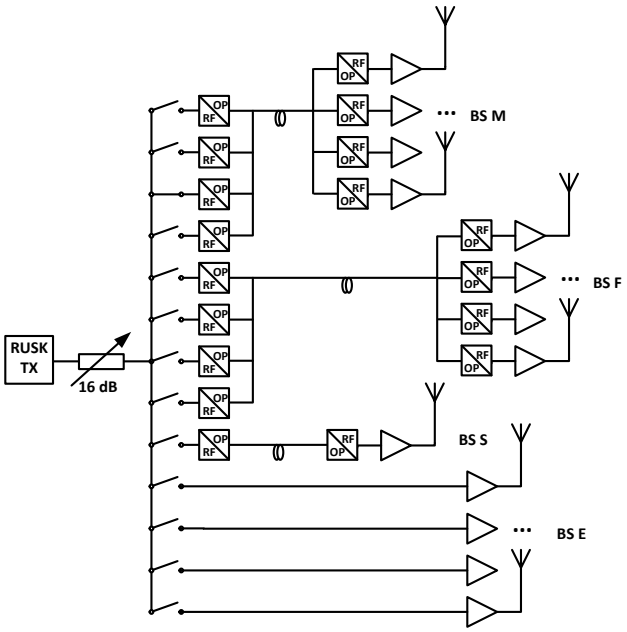

Fig. 2. Schematic diagram of the measurement setup, transmit part.

II. EXPERIMENTAL SETUP

A. Equipment

The measurement campaign was carried out with the RUSK LUND channel sounder [10] at a center frequency of 2.57 GHz and a measurement bandwidth of 40 MHz. The setup chosen consists of four transmit BSs, three of them provided with four antenna elements in a closely spaced co-polarized configuration, and one BS provided with a single antenna element. The signal broadcast by the BSs is received by a single MS equipped with 64 dual-polarized antenna elements in a uniform cylindrical array configuration. The 1664 transmit-receive channels are sounded in a time-multiplexed fashion, all of the receive antenna elements being visited in succession prior to switching to the next transmit antenna element. The data resulting from this operation is referred to as a *snapshot*. The sounding signal is conveyed to each of the remote BSs locations through the optical backbone network of the campus by means of nine OZ816 radio-over-fiber (RoF) transceivers from Optical ZONU [11], which provide a unidirectional link with operational frequencies from 47 MHz to 6.0 GHz and virtually no attenuation. In addtion, twelve Mini-Circuits ZVE-8G-7+ and one Mini-Circuits ZHL-42 power amplifiers are used at each of the transmit antenna elements, as shown in Figure 2, to raise the signal level to 30 dBm. Note that BS E is co-located with the channel sounder transmitter. For reference purposes, all parts in the setup as well as the length of the fiber links are listed in Table II. In order to account for the additional propagation delay introduced by the fibers, for which a maximum value of 8.15 μs has been estimated, a duration $T_{\text{sound}} = 12.8$ μs has been selected for the souding signal. Furthermore, an additional $3 \cdot T_{\text{sound}}$ switching time between consecutive channels is required in order to allow for the real-time recording of the data samples. Hence, a total time $T_{\text{snap}} = 85$ ms is needed for the recording of one snapshot. Each measurement *run* consists of 100 consecutive snapshots. A summary of the most important measurement parameters can be found in Table I, and a picture of one of the transmit modules with a ZONU OZ816 optical receiver unit and a Mini-Circuits ZVE-8G-7+ RF power amplifier is shown in Figure 1.

B. Antennas

Patch antenna arrays enabling two orthogonal linearly polarized excitation modes are used for both transmission and reception. The transmit antenna arrays consist of five collinear dual-polarized patch antenna elements $\lambda_c/2$ apart (ULA), tallying 8 ports. The receive antenna array is built up of four stacked uniform circular arrays (UCA), with 16 equi-spaced dual-polarized patch antenna elements on each of the UCAs, adding up to 128 ports. Let $1 \leq m \leq M_T$ consecutively run over all antenna elements in the uppermost CUA, then, in the same order, over those in the next-uppermost CUA, and so on. Equivalently, any patch antenna element m in the cylindrical array can also be referred to by a triplet (z, ϕ, i),

with $0 \leq z, \phi, i < 4$, such that the following condition holds.

$$m = 16z + 4i + \phi + 1 \tag{1}$$

Clearly, z selects one of the four UCAs, the elements of which can be grouped further into four sets indexed by ϕ. The UCAs used in the measurements posses the useful property that the joint radion pattern of the four elements belonging to one such set is approximately isotropic on the plane containing the UCA. The polarization directions of the BSs and the MS are aligned, and all unused antenna ports are loaded with 50 Ω. A picture of the transmit and receive antenna arrays is shown in Figure 1.

III. Measurement Scenario

The measurement campaign took place at the campus of Lund University, Lund, Sweden (55°42′40.00″ N, 13°12′36.61″ E), on winter of 2012 in an area which can be best characterized as semi-urban microcell environment. Four different transmit antennas were placed outside the windows at the second and third floors of four different buildings, which corresponds to 5 to 12 meters above the ground level and 10 to 20 meters below the surrounding buildings. The distances among the different antenna sites were between 60 to 200 meters. The area in the middle of the selected buildings is an open area with a small lake surrounded by high, deciduous trees. The measurements took place at four different locations, shown in Figure 3. Due to practical limitations, the measurements were performed in relatively short measurement runs, each of which comprising a straight line trajectory of 3 to 5 meters. A total of 19 measurement runs were recorded: 5 runs at each of locations Loc1, Loc2, and Loc3, as well as 4 runs at Loc4. For all of these four locations, the propagation conditions between the receiver and each of the BSs (named E, S, F and M) transmit antennas can be described as lightly obstructed line-of-sight (OLOS), where the line-of-sight (LOS) is obstructed by leafless trees and/or small concrete pillars, the only exceptions being the link between BS M and both Loc1 and Loc2, for which propagation conditions are notably non line-of-sight (NLOS).

Fig. 3. Google Map photo of the measurement campaign area. Base station locations are indicated by labels BS E, BS S, BS F and BS M. The intended measurement route is plotted in blue color.

TABLE III
Definition of the mapping BS to index l.

BS	**BS E**	**BS S**	**BS F**	**BS M**
BS index l	1	2	3	4
n	1...4	5	6...9	10...13

IV. Data Analysis

A. Preprocessing

The raw data obtained from the measurements consist of the transfer functions of the MIMO channels, which are then converted to two sets $h(t, m, n, k)$ of impulse response estimates (IREs), where the index $0 \leq t \leq 1899$ runs over the snapshots from all measurement runs, $1 \leq m \leq M_T$, $1 \leq n \leq M_R$ determine the receive antenna element and the transmit antenna element, respectively, and $0 \leq k \leq N-1$ is the delay bin index. The first set describes the vertical-to-vertical (VV) polarization propagation case, and the second one the vertical-to-horizontal (VH) case. However, in this work only the VV case is considered.

In the first place, a power correction is applied to each of the remote transmit antenna elements in order to compensate for differences in gain due to antenna arrays, amplifiers, optical transceivers and fibers. The compensation method is based on the observation that the mean path loss over a large area for two co-located transmit antenna elements must be identical. Hence, thirteen coefficients γ_n are computed as

$$\gamma_n = \frac{\sum_{t,m,n \in C(n),k} |h(t,m,n,k)|^2}{|C(n)| \cdot \sum_{t,m,k} |h(t,m,n,k)|^2} \tag{2}$$

and the IRE correction is applied according to $h_{\text{corr}}(t,m,n,k) = \gamma_n^{1/2} \cdot h(t,m,n,k)$, where $C(n)$ is the set of transmit antenna elements co-located with element n, and $|C(n)|$ denotes the number of elements in $C(n)$.

The power-corrected IREs are added coherently according to $\hat{h}(t,z,\phi,n,k) = \sum_i h_{\text{corr}}(t,z,\phi,i,n,k)$, where (1) has been used. The length of the thus-obtained IRE is then reduced by removing the bins corresponding to delays shorter than the fiber propagation time, which is different for each BS (see Table II), and considering a maximum excess delay of 3.2 μs, obtaining $\hat{h}_{short}(t,z,\phi,n,k')$, with $0 \leq k' \leq 128$. Furthermore, a thresholding algorithm is applied to each of the shortenned IREs in order to separate signal from noise. To this extent, the noise power for snapshot t is estimated as $\hat{\sigma^2}(t,l) = \mathbb{E}\left\{|\hat{h}(t,z,\phi,n,k)|^2\right\}$, where the expectation is computed as the sample mean over ϕ, z and the previously discarded delay bins, for all transmit antenna elements belonging to BS M, the one with the lowest signal-to-noise ratio (SNR).

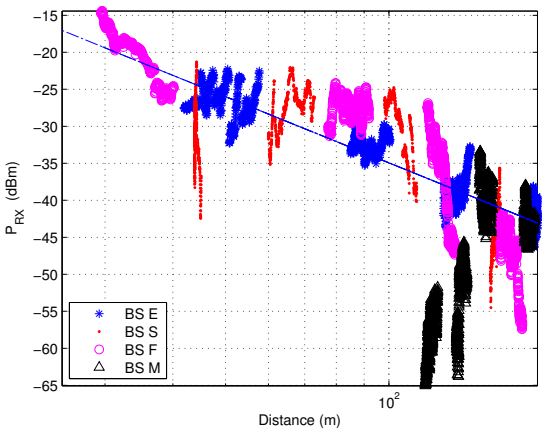

Fig. 4. Received power as a function of distance.

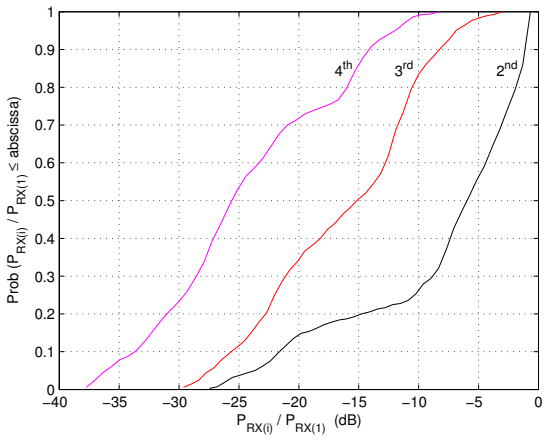

Fig. 5. Power imbalance of the received power per snapshot relative to the strongest link.

Given a snapshot t and a BS index $1 \leq l \leq 4$ as defined in Table III, a delay bin k' is classified as containing signal if $|\hat{h}_{short}(t,z,\phi,n,k')|^2 \geq \eta \cdot \hat{\sigma^2}(t,l)$ in eight or more of the samples spanned by ϕ, z and $n \in C(l)$ and, otherwise, as a noisy bin. Noisy bins are zeroed and the small-scale fading (SSF) is averaged out over ϕ, z and $n \in C(l)$ yielding $\tilde{h}^2(t,l,k')$. Finally, off-peak thresholding is applied in order to account for dynamic range limitations in the measuring system, and elements in $\tilde{h}^2(t,l,k')$ fullfilling (3) are zeroed to obtain $P_h(t,l,k')$.

$$\tilde{h}^2(t,l,k') < \zeta \cdot \max_{k'} \tilde{h}^2(t,l,k') \tag{3}$$

Threshold values of $\eta = 6$ dB and $\zeta = -35$ dB have been found suitable. The power of $P_h(t,l,k')$ averaged over k' exhibits a variation between two consecutive values of t of less than 1.32 dB in all cases and, therefore, $P_h(t,l,k')$ can be considered as the power delay profile (PDP) of the propagation channel from the receiver BS l at snapshot t.

B. Estimation of the LSF

The received power per snapshot $P_{RX}(t,l) = P_{TX}(l) \cdot \sum_{k'} P_h(t,l,k')$ is computed and the values obtained for all locations, except for those identified in Section III as NLOS, are plotted against the distance $d(t,l)$ from the receiver to BS l in double logarithmic scale, and a linear regression is performed according to (4). This is shown in Figure 4, where NLOS samples have also been included. The power decay exponent that minimizes the distance between the data samples and the line in the MMSE sense is $n = 2.95$.

$$P_{RX}(d)_{\text{dB}} = P_{RX}(d_0)_{\text{dB}} - n \cdot 10\log_{10}(\frac{d}{d_0}) \tag{4}$$

The LSF $F(t,l)$ is estimated as the difference between the received power $P_{RX}(t,l)$ and (4). The time series $F(t,l)$ is then used to analyse the correlation between the four different links in the measurement environment as detailed in Section V.

By way of illustration, the power imbalance among different links relative to the power of the strongest link is plotted in Figure 5. It can be seen, for instance, that 50% of the time the difference between the strongest and the third strongest link is less than 15 dB.

V. Discussion of Results

As explained in Section IV, the LSF was estimated as the difference between the received power and the calculated distance-dependent regression line (4) at each snapshot. The number of realizations of the LSF values is 7600 (19 runs $\times$ 100 snapshots per run $\times$ 4 BS links). The distribution of the LSF instances was found to be zero-mean log-normal with standard deviation σ = 4.58 dB.

Each measurement run results in a time series of 100 LSF values. The cross-correlation among each different pair of BS links is calculated from the corresponding time series. This results in obtaining 6 cross-correlation values from each measurement run and a total of 114 values over the whole 19 runs.

To determine whether there is a relationship between the angular difference of two BSs and the LSF cross-correlation of their links, the following steps were performed. For each measurement run, and for each pair of BS links, the absolute value of the angular difference between the BSs was calculated. Then each LSF cross-correlation value was plotted against the corresponding angular difference. The plot (which is not reported in this paper) showed no trend between the two parameters. It was found that the cross-correlation values almost span the $[-1,1]$ range regardless of the angular difference of the BSs. The calculated cross-correlation between the angular difference and the LSF cross-correlation values was found to be 0.13, which is negligible.

As it was mentioned earlier, each BS was located at different heights in different buildings. To study whether the selected location of a specific BS has a significant influence on the estimated LSF cross-correlation values between this link and the other BS links, the following steps were performed. The 114 cross-correlation values were categorized in four groups. Each group belongs to one BS and contains 57 LSF

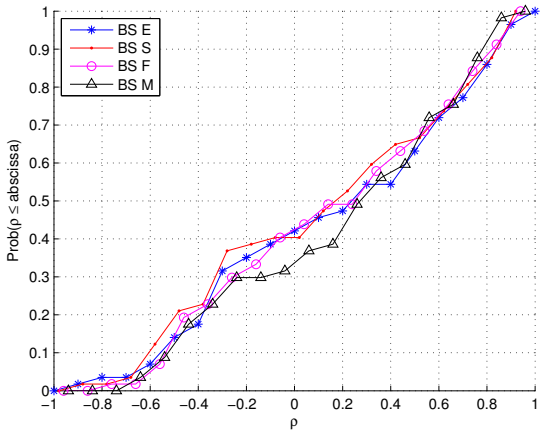

Fig. 6. CDF of the LSF cross-correlation values ρ for the different BSs.

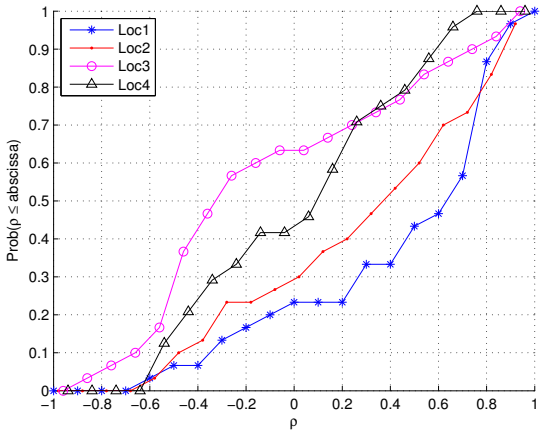

Fig. 7. CDF of the LSF cross-correlation values ρ at the different locations.

cross-correlation values representing the LSF cross-correlation values between the link of this BS and the links of the other three BSs at the different 19 runs. The CDF of each group is plotted and compared. As depicted in Figure 6, it was found that there is no significant difference among the LSF cross-correlation behaviour of the four BS links.

Finally, the 19 measurement runs were categorized into four groups, each of which representing a different measurement location. These four locations are depicted in Figure 3 and denoted by Loc1 (runs 1 to 5), Loc2 (runs 6 to 10), Loc3 (runs 11 to 15), and Loc 4 (runs 16 to 19). For each location, the LSF cross-correlation values among the four BS links (24 values for Loc4, and 30 values for each of the other locations) are grouped together. The CDFs of the cross-correlation values of the different groups were plotted and compared. As it can be concluded from Figure 7, it is clear that the LSF cross-correlation behaviour is different at the four locations. For example, there is a strong tendency of getting high negative cross-correlation values at Loc3, high positive cross-correlation values at Loc1, while the CDFs of the two other locations lie in between those of Loc1 and Loc3, with obvious difference among them. By studying the LSF cross-correlation values for the different link pairs at the 19 measurement runs (plot not included in this paper), we notice the trend of having the same cross-correlation behaviour for the majority of the link-pairs at most of the runs. This indicates that the IOs closer to MS have a higher impact on the properties of the LSF cross-correlation for different BS links. Further study is suggested in order to relate the observed LSF cross-correlation values to the physical properties of the environment local to the MS.

VI. Conclusion

Multi-site multi-antenna measurements for semi-urban microcell environment at 2.6 GHz were performed in order to study the cross-correlation properties of the LSF between different BS links in a distributed MIMO setup. The measurement setup included simultaneous transmission from four multi-antenna, distributed BSs located at different heights, and a multi-antenna MS. It was found that the angular differences between BSs, as well as the different locations of the BSs in the measurement environment have an insignificant effect on the LSF cross-correlation properties of their links. However, it was observed that the LSF cross-correlation properties of the BS links vary significantly from an MS location to another, which suggests that the IOs surrounding the MS have a higher impact on the LSF cross-correlation properties of the different links.

VII. Acknowledgements

The authors would like to acknowledge the financial support from the Swedish Foundation for Strategic Research.

References

[1] L. M. Correia, *Mobile Broadband Multimedia Networks*. Academic Press, 2006.

[2] "WINNER II channel models," tech. rep., WINNER, 2008.

[3] A. Böttcher, P. Vary, C. Schneider, and R. S. Thomä, "Cross correlation characteristics of large scale parameters in urban macro cell," in *IEEE 74th Vehicular Technology Conf.*, Sept. 2011.

[4] M. Zhu, F. Tufvesson, and J. Medbo, "Correlation properties of large scale parameters from 2.66 GHz multi-site macro cell measurements," in *IEEE 73rd Vehicular Technology Conf.*, Sept. 2011.

[5] J. Poutanen, K. Haneda, J. Salmi, V.-M. Kolmonen, F. Tufvesson, and P. Vainikainen, "Analysis of correlated shadow fading in dual-link indoor radio wave propagation," in *COST2100 9th Management Committee meeting*, 2009.

[6] J. Weitzen and T. J. Lowe, "Measurement of angular and distance correlation properties of log-normal shadowing at 1900 MHz and its application to design of PCS systems," *IEEE Trans. Veh. Technol.*, vol. 51, pp. 265–273, Mar. 2002.

[7] M. Narandžić, W. Kotterman, M. Käske, C. Schneider, G. Sommerkorn, and A. H. R. S. Thomä, "On a characterization of large-scale channel parameters for distributed (multi-link) MIMO - the impact of power level differences," in *EuCAP 4th European Conf. Antennas Propagation*, May 2010.

[8] B. L. Lau, M. A. Jensen, J. Medbo, and J. Furuskog, "Single and multi-user cooperative MIMO in a measured urban macrocellular environment," *EURASIP J. Wirel. Comm.*, vol. 2007, p. 12, Nov. 2007.

[9] V. Jungnickel, S. Jaeckel, L. Thiele, L. Jiang, U. Krüger, A. Brylka, and C. von Helmolt, "Capacity measurements in a cooperative MIMO network," *IEEE Trans. Veh. Technol.*, vol. 58, pp. 2392–2405, June 2009.

[10] R. S. Thomä, D. Hampicke, A. Richter, G. Sommerkorn, A. Schneider, U. Trautwein, and W. Wirnitzer, "Identification of time-variant directional mobile radio channels," *IEEE Trans. Instrum. Meas.*, vol. 49, pp. 357–364, Apr. 2000.

[11] "OZ816 RoF Transceiver," in *http://www.opticalzonu.com*.